

Extended-Kalman-filter-based dynamic mode decomposition for simultaneous system identification and denoising

Taku Nonomura,^{1,2} Hisaichi Shibata,³ and Ryoji Takaki³

¹⁾*Department of Aerospace Engineering, Graduate School of Engineering, Tohoku University*

²⁾*Presto, JST*

³⁾*Institute of Space and Astronautical Science, Japan Aerospace Exploration Agency*

(Dated: 4 May 2019)

A new dynamic mode decomposition (DMD) method is introduced for simultaneous system identification and denoising in conjunction with the adoption of an extended Kalman filter algorithm. The present paper explains the extended-Kalman-filter-based DMD (EKFDMD) algorithm and illustrates that EKFDMD requires significant numerical resources for many-degree-of-freedom (many-DoF) problems and that the combination with truncated proper orthogonal decomposition (trPOD) helps us to apply the EKFDMD algorithm to many-DoF problems. The numerical experiments of the present study illustrate that EKFDMD can estimate eigenmodes from a noisy dataset with a few DoF as precisely as total least squares DMD, which is a state-of-the-art algorithm for noisy data sets, whereas EKFDMD can denoise the original dataset simultaneously. The EKFDMD with trPOD can be successfully applied to many-DoF problems, including a fluid-problem example, and the results reveal the superior performance of system identification and denoising. Note that these superior results are obtained by running the proposed algorithm only once.

I. INTRODUCTION

Recently, modal decomposition¹ for fluid dynamics has attracted attention from the viewpoints of data reduction, data analysis, and reduced-order modeling of complex dataset. This is one method for data-driven science in fluid dynamics. The most conventional method of modal decomposition is a proper orthogonal decomposition (POD)^{2,3}, which is also called principal component analysis (PCA) and Karhunen-Loéve expansion. The standard POD can be computed by singular value decomposition (SVD), and this fact explains that the obtained modes are orthogonal with respect to each other. The POD modes can be computed by snapshots of fluid data and can be used for both numerical and experimental approaches. Based on the POD modes, a reduced-order model can be constructed with the Galerkin projection method for instance, although only a numerical approach can be used for reduced-order modeling in this way.

Another conventional method is global linear stability analysis (GLSA)⁴⁻⁶, which shows that the eigenmodes of the system of linearized governing equations (i.e., the Navier-Stokes equations for most of the fluid problems) around the steady state of nonlinear dynamics. Global linear stability analysis shows the most unstable eigenmodes and judges whether the steady-state solution is stable. The modes obtained by GLSA are a solution of the original linearized equations, although this method always requires numerically complex approaches and cannot be applied to experimental data. Unlike POD modes, the modes obtained by GLSA are not orthogonal.

In recent decades, a new method, dynamic mode decomposition (DMD)⁷, has been proposed and developed as a data-driven science method and has been applied to numerous fluid problems⁸⁻¹¹. Dynamic mode decomposition has characteristics of both POD and GLSA, whereas DMD can be computed only by a time-series of snapshots of numerical and experimental data. Dynamic mode decomposition processes snapshots of sequential unsteady nonlinear flow fields and yields eigenvalues and corresponding eigenmodes when the dataset is assumed to be explained by a linear system $\mathbf{x}_{k+1} = A\mathbf{x}_k$, where x_k is the k th snapshot of sequential data and A is a system matrix. These dynamic modes are generally biorthogonal, and each mode possesses a single-frequency response with amplification or damping as a natural characteristic of a linear system expression, which leads to a more intrinsic understanding of the role of each mode. Thus far, there are several methods by which to compute

the dynamic modes: the standard DMD⁷, the exact DMD, the total least squares DMD (tlsDMD)¹², the on-line DMD¹³, and the Kalman-filter-based DMD (KFDMD)¹⁴, where the latter two methods focus on the noise of the dataset. The standard DMD and the exact DMD adopt SVD and a Moore-Penrose pseudo-inverse matrix for low-rank approximation of the matrix A , respectively. This implies that these algorithms compute dynamic modes as a kind of a least-squares problem. A robust method for a noisy dataset, tlsDMD, adopts a truncated POD for pair data and successfully increases the accuracy of obtained dynamic modes. A recent KFDMD is written in the form of system identification using the Kalman filter algorithm¹⁵ and can be optimized based on the prior knowledge of the noise superimposed on the data.

However, the application of DMD to noisy data and the denoising process are still limited. One method of denoising data is the combination of tlsDMD and the sparsity-promoting DMD (spDMD). Here, spDMD¹⁶ selects finite-number modes for the reconstruction of flow fields considering the L_0 or L_1 norm of penalty terms, which is often used in sparse modeling and compressed sensing. This method is very useful for reconstructing flow fields, but the reconstructed data are governed by the initial value of the strength of each mode and possibly cannot handle the change in phase of dynamic modes in long-time data, whereas such a change is caused by nonlinear processes or sudden events in the experiments. Furthermore, the procedures to combine tlsDMD and spDMD require two-step computation. Thus far, a method for simultaneous system identification and denoising using the DMD framework has not been proposed.

In the present paper, a new method for simultaneous system identification and denoising using the DMD framework is proposed using the extended Kalman filter. In addition to the system identification of the previously proposed KFDMD¹⁴, the observed data are simultaneously filtered. The present paper first explains the algorithm of the proposed the extended-Kalman-filter-based DMD (EKFDMD). The drawback of the computational costs of EKFDMD is addressed, and combination with the truncated POD (trPOD) is proposed for the reduction of the computational cost. Finally, the proposed method is applied to various problems and its performance is illustrated.

II. KALMAN FILTER

A. Algorithm

In the present study, a discretized system in the temporal direction is adopted. As discussed above, a linear system in a vector form is considered as follows:

$$\mathbf{x}_{k+1} = A\mathbf{x}_k. \quad (1)$$

This can be written in a tensor form with the Einstein summation convention, as follows:

$$x_{i,k+1} = a_{ij}x_{j,k}. \quad (2)$$

Here, $A = (a_{ij})$, $\mathbf{x} = x_i$, and n are a system matrix, an observed variable vector, and the dimension of the observed variables, respectively. Moreover, \mathbf{x}_k is assumed to be the true value without noise.

The observed snapshot data, including noise \mathbf{y} , are defined as follows:

$$Y_{1:m} = (\mathbf{y}_m, \mathbf{y}_{m-1}, \dots, \mathbf{y}_2, \mathbf{y}_1), \quad (3)$$

whereas $\mathbf{y}_k = \mathbf{x}_k$ if the observation noise is absent.

Then, the Kalman filter algorithm is considered. In this problem, we would like to simultaneously conduct the system identification and denoising of the observed variable. Therefore, the observed variables and elements of the matrix A are chosen as state variables of the considered system. The state variable vector $\boldsymbol{\theta}$ is written as follows:

$$\boldsymbol{\theta}_k = \begin{pmatrix} \mathbf{x}_k \\ \text{vec}(A^t) \end{pmatrix} = \begin{pmatrix} x_{1,k} \\ x_{2,k} \\ \vdots \\ x_{n,k} \\ a_{11} \\ a_{12} \\ \vdots \\ a_{1n} \\ a_{21} \\ a_{22} \\ \vdots \\ a_{nn} \end{pmatrix} \quad n + n^2 \text{ dimensions.} \quad (4)$$

Using these state variables, the system transient can be written as follows:

$$\boldsymbol{\theta}_{k+1} = \begin{pmatrix} \mathbf{x}_{k+1} \\ \text{vec}(A^t) \end{pmatrix} = \mathbf{f}(\boldsymbol{\theta}_k) = \mathbf{f}(\mathbf{x}_k, A) + \mathbf{v}_k \quad (5)$$

$$\mathbf{y}_{n+1} = H\boldsymbol{\theta}_k + \mathbf{w}_k \quad (6)$$

where the \mathbf{v}_k and \mathbf{w}_k are the system and observation noise, respectively, and the nonlinear function \mathbf{f} and the observation matrix are expressed as follows:

$$\mathbf{f} = \begin{pmatrix} A\mathbf{x}_k \\ \text{vec}(A^t) \end{pmatrix} = \begin{pmatrix} a_{1j}x_{j,k} \\ a_{2j}x_{j,k} \\ \vdots \\ a_{nj}x_{j,k} \\ a_{11} \\ a_{12} \\ \vdots \\ a_{1n} \\ a_{21} \\ a_{22} \\ \vdots \\ a_{nn} \end{pmatrix}, \quad H = \overbrace{\begin{pmatrix} I & \mathbf{0} \end{pmatrix}}^{n+n^2 \text{ dimensions}}_{n \text{ dimensions}} \quad (7)$$

The upper half of the system is written as the multiplication of state variables x_j and a_{ij} , and, as such, the system is considered to be nonlinear. The lower half of the system corresponds to the constant or slowly varying system coefficients to be identified and does not change explicitly. For the construction of the extended Kalman filter, the linearization is required. The Jacobian matrix F of a nonlinear function \mathbf{f} of the state variables $\boldsymbol{\theta}$ is written as follows:

$$F_k = \frac{\partial \mathbf{f}}{\partial \boldsymbol{\theta}_k} = \begin{pmatrix} \frac{\partial A\mathbf{x}_k}{\partial \mathbf{x}_k} & \frac{\partial A\mathbf{x}_k}{\partial \text{vec}(A^t)} \\ \frac{\partial \text{vec}(A^t)}{\partial \mathbf{x}_k} & \frac{\partial \text{vec}(A^t)}{\partial \text{vec}(A^t)} \end{pmatrix} = \overbrace{\begin{pmatrix} \mathbf{x}_k^t & \mathbf{0} \\ A & \mathbf{x}_k^t \\ \mathbf{0} & \mathbf{I} \end{pmatrix}}^{n+n^2 \text{ dimensions}}_{n+n^2 \text{ dimensions}}. \quad (8)$$

(9)

Using the matrices F_k and H , the extended Kalman filter can be constructed for the nonlinear system. Note that F_k is a time-varying matrix.

Following the theory of a Kalman filter, a priori prediction of a state variable vector $\boldsymbol{\theta}_k$ and a covariance matrix $P_{k|k-1}$ can be achieved using the state variable vector $\boldsymbol{\theta}_k$ and covariance matrix $P_{k-1|k-1}$ of the previous time step,

$$\boldsymbol{\theta}_{k|k-1} = F_k \boldsymbol{\theta}_{k-1|k-1} \quad (10)$$

$$P_{k|k-1} = F_k P_{k-1|k-1} F_k^T + Q_k, \quad (11)$$

where the system matrix F_k is expressed by Eq. 9, and Q is a covariance matrix of the system noise.

When a new observation is available, the state variables and covariance matrix are updated by the Kalman gain, which is computed as

$$K_k = P_{k|k-1} H^T S_k^{-1}, \quad (12)$$

where S_k is a noise covariance matrix and is expressed as follows:

$$S_k = R_k + H P_{k|k-1} H^T. \quad (13)$$

Here, R_k is a covariance matrix of observation noise \mathbf{w}_k .

A modification vector for state variables $\boldsymbol{\theta}$ is computed as follows:

$$\delta\boldsymbol{\theta}_{k|k} = K_k (\mathbf{y}_k - H \boldsymbol{\theta}_{k|k-1}) \quad (14)$$

$$= K_k (\mathbf{y}_k - A_{k|k-1} \mathbf{x}_{k-1|k-1}). \quad (15)$$

Finally, the state variable vector and the covariance matrix after the observation are updated as follows:

$$\boldsymbol{\theta}_{k|k} = \boldsymbol{\theta}_{k|k-1} + \delta\boldsymbol{\theta}_{k|k}. \quad (16)$$

$$P_{k|k} = (I - K_k H) P_{k|k-1}. \quad (17)$$

This extended Kalman filter requires the inversion of the large matrix S_k with dimension of n^2 . This is a clear drawback of this formulation for many-degree-of-freedom(DoF) problems, and using this algorithm together with trPOD is recommended, as explained in Section II B. This drawback of EKFDM is the same as that of KFDMD for only the system identification, whereas the drawback of KFDMD is somehow relaxed owing to the fast

algorithm proposed in the previous study¹⁴, in which the large matrix is assumed to be decomposed into several block matrices being identical to each other. Although we attempt to use a concept similar to the previous KFDMD¹⁴, we could not find a similar method for the present formulation. Therefore, the situation of EKFDM is severer than that of KFDMD for only system identification, and the use of the present algorithm together with trPOD is strongly recommended for many-DoF problems.

B. Combination with the truncated POD

As discussed in the previous section, the computational cost of the present algorithm is high, and, therefore, the truncated POD (truncated SVD) is used in conjunction with a reduction in the number of DoF of the dataset of the observed variables. Similar to a previous study on KFDMD for only system identification, the obtained data are processed as follows:

1. the batch POD is applied,
2. a proposed Kalman filter is then applied to the amplitude of each POD mode, and
3. the mode shape of a fluid system is finally recovered by multiplying the spatial POD modes.

As the first step (step 1), POD is applied to an observed data matrix and an observed data matrix is expressed in SVD form as follows:

$$Y_{1:m} = U_{1:m} D_{1:m} V_{1:m}^t. \quad (18)$$

Here, U and V are matrices consisting of the spatial and temporal POD modes, respectively. The r -rank approximation of the observed data matrix is calculated as follows:

$$Y_{1:m} \sim \tilde{U}_{1:m} \tilde{D}_{1:m} \tilde{V}_{1:m}^t, \quad (19)$$

where quantities with tildes indicate r -rank approximations. Here, the r -dimension matrix of \tilde{D} consists of r -largest singular values of D . In addition, the row vectors of \tilde{U} and \tilde{V} are the same as the corresponding first r row vectors of U and V . Using these matrixes, reduced-order \tilde{Y} , which represents mode strength, is constructed as follows:

$$\tilde{Y}_{1:m} = \tilde{D}_{1:m} \tilde{V}_{1:m}^t. \quad (20)$$

In the second step (step 2), \tilde{Y} and \tilde{y}_k are treated in a manner similar to Y and y_k in the proposed EKFDMD procedures, and \mathbf{x}_k and A are simultaneously estimated. In addition, for the online implementation,

$$\tilde{y}_k = \tilde{U}^t y_k \quad (21)$$

can be used where the left singular vector is assumed to be fixed using the sample data. After this process, the eigenvalues and eigenmodes are computed by solving the eigenvalue problem of A .

Finally, in the third step (step 3), the original dimension of the eigenmode is obtained by multiplying the matrix U after obtaining the right eigenvector of the reduced system by EKFDMD.

In the present paper, Eq. 20 is adopted for the truncated POD. This procedure is used for many-DoF problems ($n > 30$) and is not used unless otherwise mentioned.

III. NUMERICAL EXPERIMENTS AND DISCUSSION

The EKFDMD algorithm described in Section II A is adopted in the numerical experiments below.

A. Problem with a small number of DoF

First, the performance of EKFDMD is investigated for the standard problem, in comparison with the standard DMD, KFDMD, and tlsDMD. The methods and dataset are the same as those of the previous study¹² and only the observation noise is considered in the present study. The eigenvalues are set to be at $\lambda_1 = \exp(\pm 2\pi i \Delta t)$, $\lambda_2 = \exp(\pm 5\pi i \Delta t)$, and $\lambda_3 = \exp[(-0.3 + 11\pi i) \Delta t]$, where $\Delta t = 0.01$. The DoF of this system becomes $d = 6$ but is expanded to snapshot data of $r = 16$ DoF by applying QR decomposition. Note that this problem was originally extended to $r = 400$ DoF but the number of DoF is limited in the present study because of the computational costs of EKFDMD, as mentioned above. In this process, a random matrix T of the $r \times d$ dimensions is transformed into $T = QR$ by QR decomposition, and the original data \mathbf{f} of dimension d are extended to \mathbf{x} of dimension r by multiplication by the matrix Q . When the noisy data are considered, y data matrixes are created by adding white observation noise to the original x data matrix, where the noise is

expressed as $\mathcal{N}(0, \sigma^2)$. The variance (σ^2) is set to be 0.1, which results in very noisy data (see the “data” and “noisy data” in Fig. 4). A total of 200 snapshots are given, and the eigenvalues of the matrix A in the final stage are analyzed.

For the initial adjustable parameters of the Kalman filter, the diagonal parts of the covariance matrix are set to be 10^3 . The diagonal elements of R and Q are set to be 0.1, and 0, respectively, and the nondiagonal elements of them are set to be 0. Here, \mathbf{x} is overwritten by \mathbf{y} , and only the matrix A is estimated for the initial 100 time steps, after which simultaneous identification and denoising are started. This initial treatment is very important in order to prevent the divergence of the algorithm.

First, the data without noise are processed, and the eigenvalue results are discussed. Figure 1 shows the eigenvalues obtained from the standard DMD, KFDMD, tlsDMD, and EKFDMD. Figure 1 shows that the results of all of the methods adopted here, i.e., the standard DMD, KFDMD, tlsDMD, and EKFDMD, agree well with the true values, suggesting that all of the algorithms provide accurate estimations of the eigenvalues under the condition without noise.

Then, the results based on the noisy data are discussed. Figures 2 and 3 show the eigenvalues estimated in the representative case and in all of the 100 cases we examined by changing the random number seed, respectively. The results of the estimated eigenvalues in Figs. 2 and 3 show that DMD and KFDMD do not work well for the accurate estimation of the eigenvalues of the system. On the other hand, both tlsDMD and EKFDMD work well for the estimation of eigenvalues. This might be because EKFDMD denoises the data, and a more accurate eigenvalue of the system can be obtained by the denoised data. The system identification performance of EKFDMD appears to be as good as that of tlsDMD. Note that the eigenvalues of DMD and tlsDMD are not scattered in the region of less than 0.5 of their real parts, because the number of DoF is reduced to six by the trPOD, which is inherently involved in the original algorithms of these methods, and that the eigenvalues of KFDMD and EKFDMD are scattered in the region because no trPOD is applied for 16 DoF, and spurious oscillations remain. If we apply the trPOD to the data matrix as a preconditioner and limit the number of DoF to be six, then the scattered eigenvalues can also be removed for KFDMD and EKFDMD.

In addition, as noted previously, EKFDMD is expected to be able to denoise the data. Figure 4, which illustrates the time-series of data with/without noise and the EKFDMD

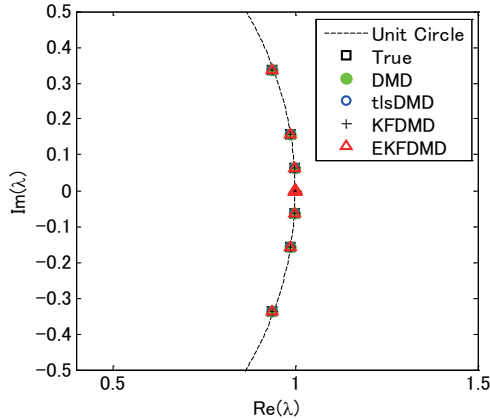


FIG. 1. Eigenvalues for a problem with a small number of DoF without noise.

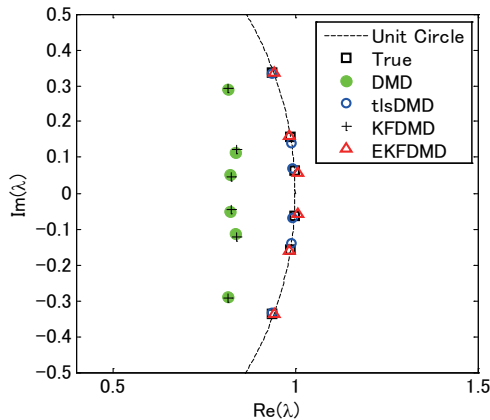


FIG. 2. Eigenvalues for a problem with a small number of DoF with noise.

denoised results, reveals that EKFDMD can successfully denoise the data, although the noise level is very high. Similar results might be obtained through the combination of spDMD and tlsDMD, but EKFDMD provides the denoised data and identified system coefficients by running the algorithm only once.

B. Problem with a moderate number of DoF

Next, a similar problem, but with the number of DoF extended to 200 by the same procedure, is adopted with the same noise level. In this case, the computational cost is very high, and we conducted trPOD as a preconditioner. In this problem, first, the number of DoF is reduced from 200 to 12 by trPOD, and the reduced data are processed in EKFDMD. On the other hand, for the purpose of comparison, DMD and tlsDMD are applied directly

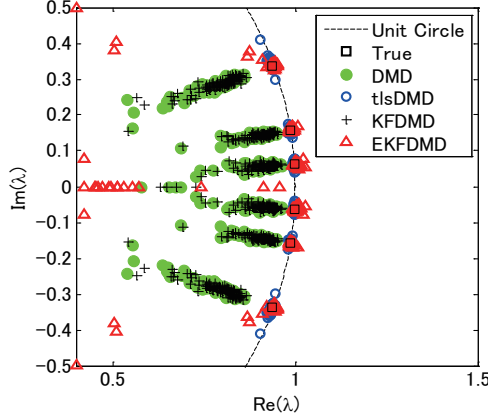


FIG. 3. Eigenvalues for multiple runs of a problem with a small number of DoF with noise, where the random seed or noise generation is different for multiple runs.

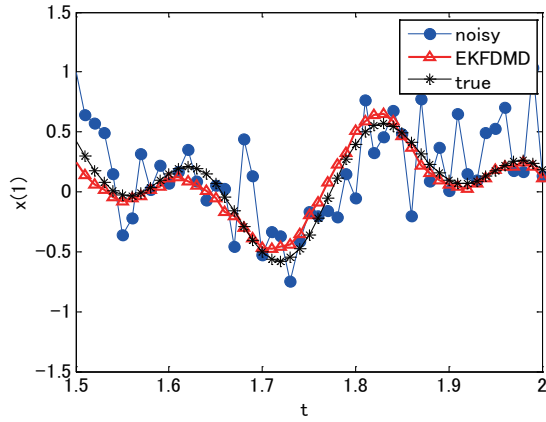


FIG. 4. Time history of the first node of the data for a problem with a small number of DoF.

to the 200 DoF data in order to reduce the number of DoF to 12 because these algorithms can treat a data matrix of this size within a reasonable computational time by inherently involving truncated SVD (same as trPOD). Here, KFDMD is not applied to this problem, because KFDMD shows similar results as the standard DMD in the present situation, in which the noise level does not change over time, as shown in the previous problem. In this problem, 1,600 samples were given, and \mathbf{x} is overwritten by \mathbf{y} in the first 100 samples, which is similar to the previous problem. Note that we also considered 200 to 800 samples, although 1,600 samples provided better results. This might be explained by two factors: 1) the trPOD modes are improved by using more samples, and 2) the KFDMD estimation is improved by using more samples. Similar to the previous example, the diagonal elements of

the covariance matrix are set to be 10^3 in the initial condition. The diagonal elements of R and Q are set to be 0.1 and 0, respectively, and the nondiagonal elements of them are set to be 0.

The results of trPOD are shown in Fig. 5, where the first POD spatial mode obtained by data without noise and those obtained by data with noise are plotted together; note that the mode of the node distribution in snapshots is referred to as the POD spatial mode in analogy to fluid analysis. This plot shows that the noise level is very high and the estimation of the POD spatial mode is not accurate. However, the contaminated POD modes obtained by data with noise are used for EKFDMD.

The results of eigenvalues in the representative case, and in all 100 cases we considered, by changing the random seed (similar to the previous problem), are shown in Figs. 6 and 7, respectively. The results for the estimated eigenvalues in Figs. 6 and 7 exhibit a similar trend to those observed for the previous problem: the eigenvalues of DMD and KFDMD are not sufficiently accurate, but those of tlsDMD and EKFDMD are sufficiently accurate. As noted above, 12 DoF are left for all of the algorithms, i.e., DMD, tlsDMD, and EKFDMD, by using truncated POD, which is inherently used for the standard DMD and tlsDMD and is used as a preconditioner for EKFDMD. Although the POD spatial mode is not accurate, as shown above, the eigenvalue of the system is estimated by EKFDMD to be sufficiently accurate.

In addition, the EKFDMD can denoise the data of the POD mode and an original node, as shown in Figs. 8 and 9, in which the given and processed time series data of the first POD mode and the first node of the dataset are shown. Figures 8 and 9 show that EKFDMD can denoise the temporal behavior of the data successfully. This might lead to the accurate estimation of the eigenvalue of the system.

C. Application to fluid problem

The simulation of a two-dimensional flow around a cylinder is conducted. The Mach number of the freestream velocity is set to be 0.3, and the Reynolds number based on the freestream velocity and the cylinder diameter is set to be 300. For the analysis, LANS3D¹⁷, which is an in-house compressible fluid solver, is adopted. A cylindrical computational mesh is used, with the numbers of the radial- and azimuthal-direction grid points being

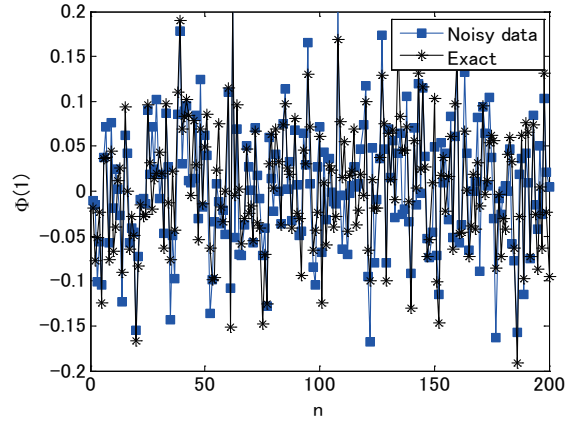


FIG. 5. First POD mode of original and noisy data for a problem with a moderate number of DoF.

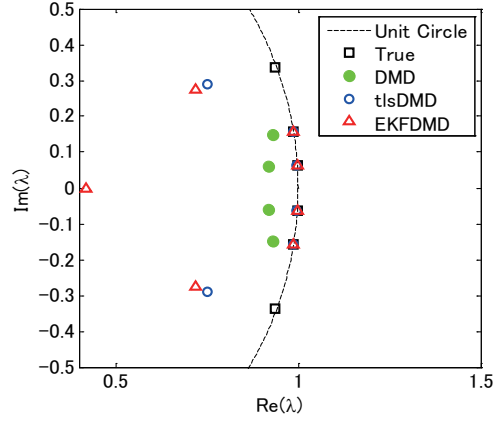


FIG. 6. Eigenvalues for a problem with a small number of DoF with noise.

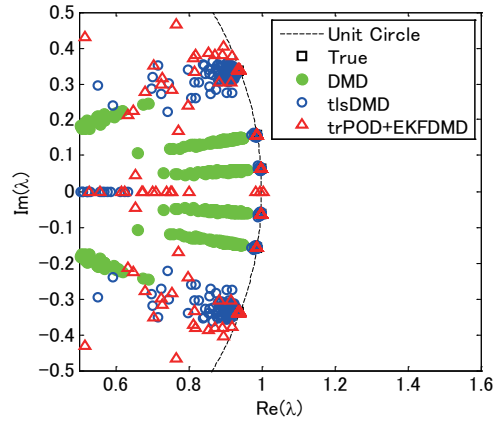


FIG. 7. Eigenvalues for multiple runs of a problem with a moderate number of DoF with noise.

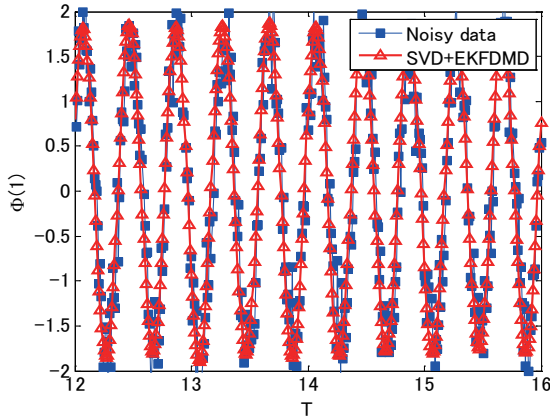


FIG. 8. Time history of the first node of the data for a problem with a moderate number of DoF.

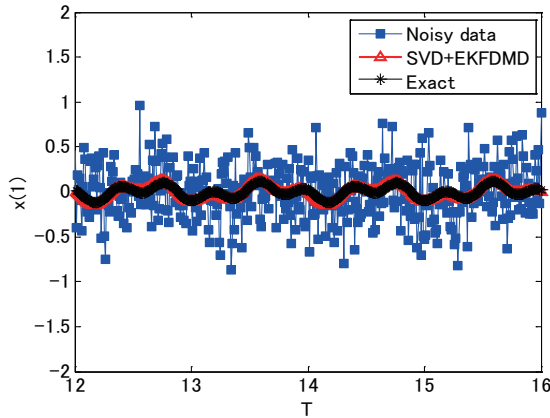


FIG. 9. Time history of the first mode of the data for a problem with a moderate number of DoF.

250 and 111, respectively. A compact difference scheme¹⁸ of the sixth order of accuracy is used for spatial derivatives and a second-order backward differencing scheme converged by an alternative-directional-implicit symmetric-Gauss-Seidel method^{19,20} is used for time integration. See Reference²¹ for further details. The origin point is set to be the center of the cylinder, and a resolved region (where it is fine mesh density) is set to be inside $10d$ far from the origin point. Here, d is the diameter of the cylinder. For any DMD analyses, the quasi-steady flow data at $x = [0, 10d]$, $y = [-5d, 5d]$, which is in the wake region, are used. The data are mapped to an equally distributed 100×100 mesh. The DMD analyses processed 500 samples of five flow-through data with or without adding observation noise of $\mathcal{N}(0, \sigma^2)$, whereas the variance (σ^2) is set to be 0.02. In EFKDDMD algorithm, the diagonal parts of the covariance matrix are initially set to be 10^3 similar to the previous problems.

The diagonal elements of R and Q are set to be 0.02, and 0, respectively, while nondiagonal elements of them are set to be 0.

First, the results without noise are processed by DMD and KFDMD, where KFDMD adopts the truncated POD (Eq. 20) as a preconditioner. The eigenvalues computed by the DMD and KFDMD methods are shown in Fig. 12. The eigenvalues computed by KFDMD agree well with those of the standard DMD. The lowest frequencies computed by DMD and KFDMD correspond to the Strouhal number $St = fd/u_\infty \sim 0.2$, which is a well-known characteristic frequency for the Kármán vortex street of a cylinder wake, where f and u_∞ are the frequency and the freestream velocity, respectively.

The snapshot data of the instantaneous flow field are shown in Fig. 10. Flow fields filtered using only trPOD are shown in Fig. 11. The noise can be reduced using trPOD. These 30 DoF data are used for the DMD, trDMD, and KFDMD analyses.

First, the flow field without noise is processed by DMD, tlsDMD, and EKFDMD. Figure 12 shows that the eigenvalues obtained by these algorithms coincide with each other, and the eigenvalues of this problem are on a unit circle, which shows the Kármán vortex is shed periodically.

Then, the data with noise are processed. Figure 13, which illustrates the eigenvalues of DMD, tlsDMD, and EKFDMD, shows that the EKFDMD results are better than the results of the standard DMD and predicts from the steady flow mode (eigenvalue of unity) to the fourth oscillation mode, which corresponds to nine points on the unit circle. On the other hand, Fig. 13 shows that tlsDMD works better than EKFDMD. This might be because the trPOD preconditioner does not work as well as that of tlsDMD for a limited number of samples. This point should be improved in a future study. However, note that the strength of EKFDMD is that the data are denoised simultaneously. Figure 14 shows the mode histories of trPOD modes 2, 4, 6, and 8. The histories of modes 2 and 4 are approximately the same for noisy data and EKFDMD combined with the trPOD preconditioner, because these modes are strong enough compared with the noise level. On the other hand, the histories of modes 6 and 8 are cleaned up well. Finally, the flow fields of denoised data (in this case, the temporal coefficients of the trPOD modes are filtered) are shown in Fig. 15 and the data are slightly further cleaned up compared to the results obtained with only trPOD shown in Fig. 11.

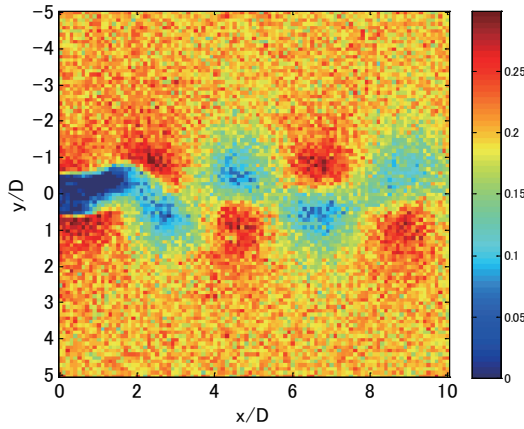


FIG. 10. Noisy flow field data processed by several DMD methods. The x -direction velocity is visualized, where the freestream velocity is set to be 0.3.

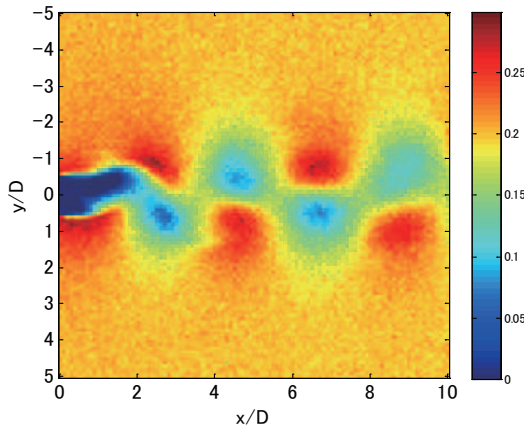


FIG. 11. trPOD 30 mode reconstruction of flow fields. The x -direction velocity is visualized, where the freestream velocity is set to be 0.3.

IV. CONCLUSIONS

A dynamic mode decomposition method based on the extended Kalman filter (EKFDMD) was proposed for simultaneous parameter estimation and denoising. The numerical experiments of the present study reveal that the proposed method can estimate the eigenstructure of the matrix A as precisely as the tlsDMD problem, whereas EKFDMD denoises the data by running the algorithm only once, for a problem with a small number of DoF. However, this algorithm has the drawback of computational cost. This drawback is addressed by the preconditioning of truncated POD (trPOD), and EKFDMD with trPOD is applied to a

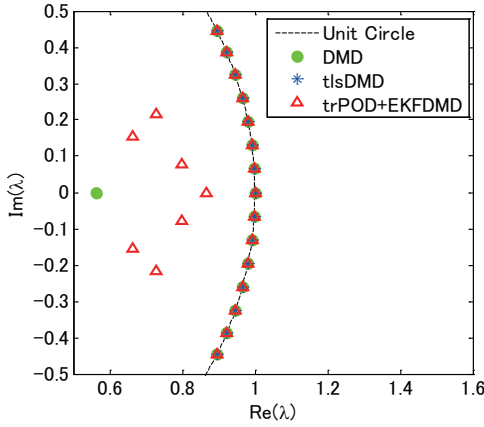


FIG. 12. Eigenvalues for a flow problem without noise.

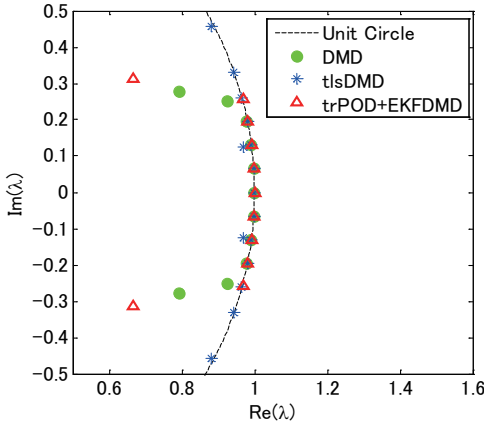
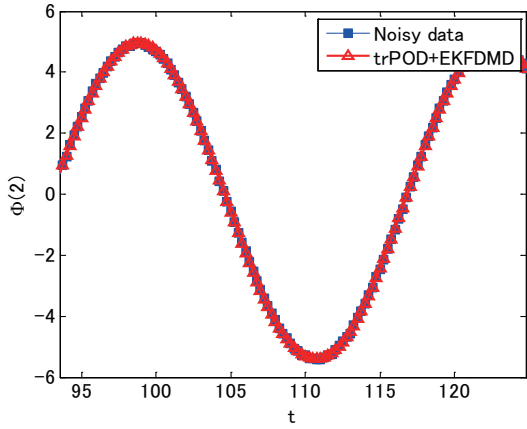


FIG. 13. Eigenvalues for a flow problem with noise.

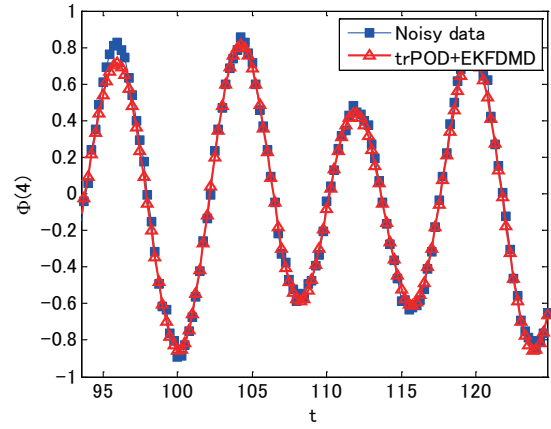
problem with a moderate number of DoF and a fluid system. The accuracy of eigensystem estimation of EKF DMD appears to be better than the standard DMD, but is approximately the same as that of the tlsDMD. The data filtered by EKF DMD appear to be well denoised. Note that all of these properties are preferable in the analysis of noisy data.

REFERENCES

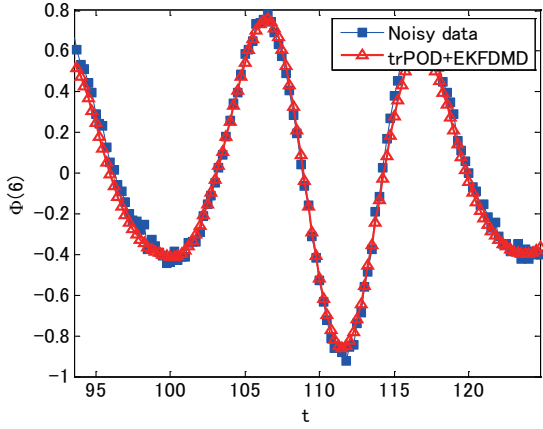
¹Kunihiko Taira, Steven L. Brunton, Scott T. M. Dawson, Clarence W. Rowley, Tim Colonius, Beverley J. McKeon, Oliver T. Schmidt, Stanislav Gordeyev, Vassilios Theofilis, and Lawrence S. Ukeiley, “Modal Analysis of Fluid Flows: An Overview,” , 1–46(2017), arXiv:1702.01453, <http://arxiv.org/abs/1702.01453>.



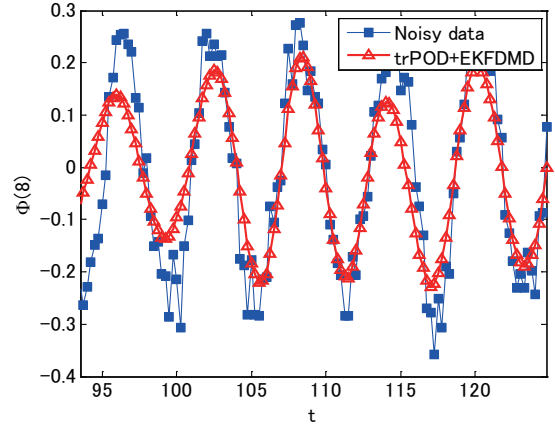
(a) mode 2



(b) mode 4



(c) mode 6



(d) mode 8

FIG. 14. Time history of POD modes 2, 4, 6, and 8 of the data of the flow problem.

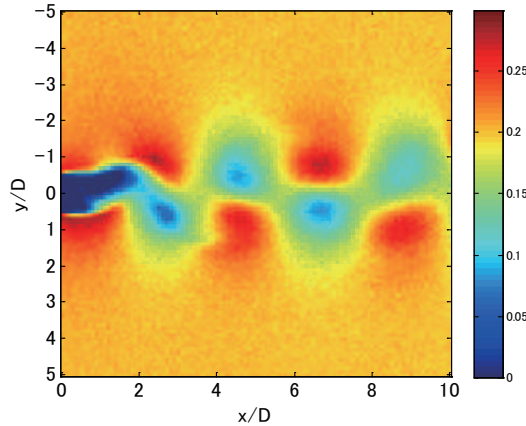


FIG. 15. EKFDDMD-filtered flow fields. The x -direction velocity is visualized, where the freestream velocity is set to be 0.3.

²Clarence W. Rowley, Tim Colonius, and Richard M. Murray, “Model reduction for compressible flows using POD and Galerkin projection,” *Physica D: Nonlinear Phenomena* **189**, 115–129 (2004), ISSN 01672789.

³Gal Berkooz, Philip Holmes, and L. John Lumley, “The proper orthogonal decomposition in the analysis of turbulent flows,” *Annual Review of Fluid Mechanics* **25**, 539–575 (1993), ISSN 0066-4189, <http://citeserx.ist.psu.edu/viewdoc/download?doi=10.1.1.212.4071&rep=rep1&type=pdf>

⁴Vassilios Theofanis, “Global Linear Instability,” *Annual Review of Fluid Mechanics* **43**, 319–352 (2011), ISSN 0066-4189.

⁵H. Shibata, Y. Ohmichi, Y. Watanabe, and K. Suzuki, “Global stability analysis method to numerically predict precursor of breakdown voltage,” *Plasma Sources Science and Technology* **24** (2015), ISSN 13616595 09630252, doi: “bibinfo doi 10.1088/0963-0252/24/5/055014.

⁶Yuya Ohmichi and Kojiro Suzuki, “Assessment of global linear stability analysis using a time-stepping approach for compressible flows,” *International Journal for Numerical Methods in Fluids* **80**, 614–627 (2016), ISSN 02712091, arXiv:fld.1 [DOI: 10.1002], <http://doi.wiley.com/10.1002/fld.4166>.

⁷P. J. Schmid, “Dynamic mode decomposition of numerical and experimental data,” *Journal of Fluid Mechanics* **656**, 5–28 (2010), ISSN 0022-1120, arXiv:arXiv:1312.0041v1.

⁸Jonathan H. Tu, Clarence W. Rowley, Dirk M. Luchtenburg, Steven L. Brunton, and J. Nathan Kutz, “On dynamic mode decomposition: Theory and applications,” *Journal of Computational Dynamics* **1**, 391–421 (2014), ISSN 2158-2491, arXiv:1312.0041, <http://www.aimsceances.org/journals/displayArticlesnew.jsp?paperID=10631>.

⁹Lei Wang and Li-Hao Feng, “Extraction and Reconstruction of Individual Vortex-Shedding Mode from Bistable Flow,” *AIAA Journal*, 1–13(2017), ISSN 0001-1452, <https://arc.aiaa.org/doi/10.2514/1.J055306>.

¹⁰Stephan Priebe, Jonathan H. Tu, Clarence W. Rowley, and M. Pino Martín, “Low-frequency dynamics in a shock-induced separated flow,” *Journal of Fluid Mechanics* **807**, 441–477 (2016), ISSN 0022-1120, http://www.journals.cambridge.org/abstract_S0022112016005577.

¹¹Yuya Ohmichi, Takashi Ishida, and Atsushi Hashimoto, “Numerical Investigation of Transonic Buffet on a Three-Dimensional Wing using Incremental Mode Decomposition,” 55th AIAA Aerospace Sciences Meeting, 1–8(2017),

<http://arc.aiaa.org/doi/10.2514/6.2017-1436>.

¹²Maziar S. Hemati, Clarence W. Rowley, Eric A. Deem, and Louis N. Cattafesta, “De-biasing the dynamic mode decomposition for applied Koopman spectral analysis of noisy datasets,” *Theoretical and Computational Fluid Dynamics*, 1–20(2017), ISSN 14322250, 1502.03854.

¹³Hao Zhang, Clarence W. Rowley, Eric A. Deem, and Louis N. Cattafesta, “Online dynamic mode decomposition for time-varying systems,” , 1–22(2017), arXiv:1707.02876, <http://arxiv.org/abs/1707.02876>.

¹⁴Taku Nonomura, Hisaich Shibata, and Ryoji Takaki, “Dynamic mode decomposition using a kalman filter for parameter estimation,” , 1–20(2018), arXiv:1804.00143, <http://arxiv.org/abs/1804.00143>.

¹⁵R. E. Kalman, “A New Approach to Linear Filtering and Prediction Problems,” *Journal of Basic Engineering* **82**, 35 (1960), ISSN 00219223, <http://scholar.google.com/scholar?hl=en&btnG=Search&q=intitle:A+New+Approach+to+Lin>

¹⁶Mihailo R. Jovanović, Peter J. Schmid, and Joseph W. Nichols, “Sparsity-promoting dynamic mode decomposition,” *Physics of Fluids* **26**, 1–22 (2014), ISSN 10897666, arXiv:arXiv:1309.4165v1.

¹⁷K. Fujii, H. Endo, and M. Yasuhara, “Activities of computational fluid dynamics in japan: Compressible flow simulations,” *High Performance Computing Research and Practice in Japan*, Wiley Professional Computing, JOHN WILEY& SONS, 139–161(1990).

¹⁸Sanjiva K. Lele, “Compact finite difference schemes with spectral-like resolution..” *Journal of Computational Physics* **103**, 16–42 (1992).

¹⁹Kozo Fujii, “Efficiency improvement of unified implicit relaxation/time integration algorithms,” *AIAA Journal* **37**, 125–128 (1999).

²⁰Hiroyuki Nishida and Taku Nonomura, “Adi-sgs scheme on ideal magnetohydrodynamics,” *Journal of Computational Physics* **228**, 3182–3188 (2009).

²¹Makoto Sato, Taku Nonomura, Koichi Okada, Kengo Asada, Hikaru Aono, Aiko Yakeno, Yoshiaki Abe, and Kozo Fujii, “Mechanisms for laminar separated-flow control using dielectric-barrier-discharge plasma actuator at low reynolds number,” *Physics of Fluids* **27**, 1–29 (2015).